

Analysis of Butt Coupling in Photonic Crystals

Pablo Sanchis, *Student Member, IEEE*, Peter Bienstman, *Associate Member, IEEE*, Bert Luyssaert, *Member, IEEE*, Roel Baets, *Senior Member, IEEE*, and Javier Marti, *Member, IEEE*

Abstract—We present a detailed analysis of butt coupling from conventional dielectric waveguides into photonic crystal waveguides. Closed-form expressions for the reflection and transmission matrices based on an eigenmode expansion technique are derived and validated by means of simulations. We use them to investigate butt-coupling losses in two kinds of photonic crystal structures: one formed by rods with a higher refractive index than the surrounding medium and the other formed by air holes inserted in a high-refractive-index medium. The origin and difference of coupling losses between the two photonic crystal structures is analyzed and discussed. We show that, although the coupling efficiency is much worse in the former structure, it can be significantly improved by choosing the optimum interface position that minimizes the mode impedance mismatch. Furthermore, the dependence of coupling efficiency on frequency is also analyzed. Finally, we also relate some traditionally used approximate formulas to our rigorous expressions.

Index Terms—Electromagnetic scattering by periodic structures, optical propagation in nonhomogeneous media, periodic structures.

I. INTRODUCTION

IN RECENT years, all-optical networks have been the subject of a significant research effort in order to address the increasing data traffic. Micro-scale photonic integrated circuits are key components in these kinds of networks to avoid the bottleneck introduced by current components performed in the electronic domain. Photonic crystal circuits are expected to be one of the main candidates for the realization of photonic integrated circuits because of their ability to control the flow of light on a small scale [1]. Therefore, the interest in these circuits has grown exponentially since they were initially proposed by Yablonovitch and John in 1987 [2], [3].

Efficient coupling into photonic crystal circuits is a key step for the definitive commercial deployment of this technology. Coupling losses are due to the different features and guiding mechanism in both waveguides. Waveguides in photonic crystal

circuits are usually formed by inserting line defects into the otherwise periodic structure. Propagation in these kinds of waveguides is characterized by Bloch modes. On the other hand, propagation in conventional dielectric waveguides relies on index-contrast guiding. A large variety of coupling techniques and structures have recently been proposed for efficient interfacing fiber and wide dielectric waveguides to the narrower photonic crystal waveguide. Among all of them, photonic crystal tapers are a promising approach due to the small coupling length and high coupling efficiencies achieved in a broad frequency range [4]–[9]. However, an efficient interfacing between dielectric and photonic crystal waveguides with a similar width may also be important if photonic crystal circuits have to be inserted on a chip with other blocks relying on traditional index-contrast guiding.

Butt-coupling losses are rather different depending on the nature of the photonic crystal considered. In rod photonic crystal structures, where the photonic crystal is formed by rods with a higher refractive index than the surrounding medium, the coupling efficiency is in general poor [10], [11]. However, in hole photonic crystal structures, where the photonic crystal is formed by air holes inserted in a high refractive index medium, the coupling efficiency is very high and transmission efficiencies near 100% can be achieved [12]–[15]. Coupling losses in both kinds of photonic crystal structures have been studied by means of simulations, but to the best of our knowledge there has not been any systematic, all-encompassing analytic study at the moment.

The aim of this paper is to obtain analytic expressions for the reflection and transmission matrices at an interface formed by a dielectric waveguide butt coupled to a photonic crystal waveguide. Closed-form expressions are obtained based on an eigenmode expansion technique and a Bloch basis. The Bloch mode basis has been used for engineering gratings, propagation in finite photonic crystal waveguides, or taper transitions in photonic crystals [16]–[20]. In this paper, the coupling from a dielectric waveguide into a semi-infinite photonic crystal waveguide is considered. The usefulness of the classical approximate formula employed to study fiber-coupling issues is also analyzed.

We use analytic expressions, validated by means of simulations, to study coupling losses in both rod and hole photonic crystal structures to get a qualitative insight in the origin of coupling losses. As already mentioned, coupling losses in the rod structure are much higher than in the hole structure. This difference is determined by the properties of the Bloch modes that can be quite different depending on the features of the photonic crystal. However, transmission efficiency can be significantly improved by using the optimum interface between the dielectric and photonic crystal waveguide. The optimum interface is obtained among the different cuts that can be chosen within the basic period of the photonic crystal. Furthermore, we show that

Manuscript received November 14, 2003; revised January 26, 2004. This work was supported in part by the Spanish Ministry of Science and Technology under Grant TIC2002-01553. Parts of this work were also performed in the context of the Belgian DWTC Project IAP-Photon. The work of P. Sanchis was supported by the Spanish Ministry of Education, Culture and Sport. The work of P. Bienstman was supported by the Flemish Fund for Scientific Research (FWO-Vlaanderen) through a postdoctoral fellowship. The work of B. Luyssaert was supported by the Flemish Institute for the Industrial Advancement of Scientific and Technological Research (IWT) through a specialist grant.

P. Sanchis and J. Marti are with the Fiber-Radio Group, Nanophotonics Technology Center, Universidad Politécnic de Valencia, 46022 Valencia, Spain (e-mail: pabsanki@upvnet.upv.es).

P. Bienstman, B. Luyssaert, and R. Baets are with the Department of Information Technology, Interuniversity Micro-Electronics Centre (IMEC), Ghent University, B-9000 Ghent, Belgium.

Digital Object Identifier 10.1109/JQE.2004.826428

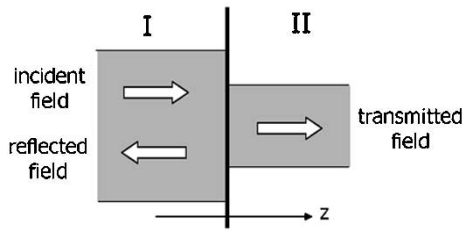


Fig. 1. Interface between two media.

even choosing the optimum interface the maximum transmission will be limited by the group velocity mismatch that exists between the dielectric and photonic crystal waveguide. However, we obtain that the transmission efficiency can increase from values lower than 5% to values near 70% for the rod structure while efficiency near 100% can be achieved for the hole structure in a broad frequency range by choosing the optimum interface.

The paper is structured as follows. In Section II, we briefly review the procedure to derive the transmission and reflection matrices at an interface between two dielectric waveguides. This approach is generalized in Section II to derive the transmission and reflection matrices for an interface between a dielectric and a photonic crystal waveguide. Two different approaches are provided. Analytic results are then compared with simulations in Section IV and the difference in coupling losses between a rod and a hole photonic crystal structures are analyzed and discussed. Finally, conclusions are drawn in Section V.

II. INTERFACE BETWEEN TWO DIELECTRIC WAVEGUIDES

Fig. 1 shows the interface between two different media where the z axis is oriented along the propagation direction. In this case, we consider that both media are z -invariant. If the interface is placed at $z = 0$ and a single mode with index p is incident from medium I, this incident mode will give rise to a reflected field in medium I and a transmitted field in medium II. The following derivation is based on the well-known mode-matching technique [21], [22]. We expand the fields in terms of the eigenmodes of each medium and impose the continuity of the tangential components of the total field

$$E_p^I + \sum_j R_{j,p} E_j^I = \sum_j T_{j,p} E_j^II \quad (1)$$

$$H_p^I - \sum_j R_{j,p} H_j^I = \sum_j T_{j,p} H_j^II \quad (2)$$

where E, H are the electric and magnetic tangential fields, respectively, and T and R are the transmission and reflection coefficients, respectively. The minus sign of the reflected magnetic field is due to the symmetries for the backward propagating modes. In order to calculate the unknown transmission and reflection coefficients, we take the right cross product of (1) with H_I^I and the left cross product of (2) with E_I^I , which are the expansion fields of medium I. Here, i is an arbitrary index. After integrating over the cross section, we get

$$\langle E_p^I, H_I^I \rangle + \sum_j R_{j,p} \langle E_j^I, H_I^I \rangle = \sum_j T_{j,p} \langle E_j^II, H_I^I \rangle \quad (3)$$

$$\langle E_I^I, H_p^I \rangle - \sum_j R_{j,p} \langle E_I^I, H_j^I \rangle = \sum_j T_{j,p} \langle E_I^I, H_j^II \rangle \quad (4)$$

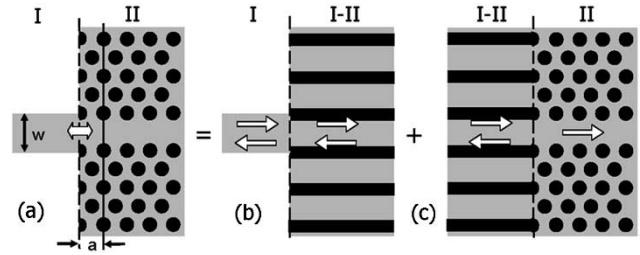


Fig. 2. Schematic of the analyzed structures where w is the width of the input waveguide and a is the lattice constant.

where the scalar product is defined as the following overlap integral:

$$\langle E_n, H_m \rangle = \iint_S (E_n \times H_m) \cdot u_z dS.$$

By invoking the orthogonality relation and after some algebraic manipulations, we obtain

$$2\delta_{Ip} \langle E_p^I, H_p^I \rangle = \sum_j T_{j,p} [\langle E_j^II, H_I^I \rangle + \langle E_I^I, H_j^II \rangle] \quad (5)$$

$$R_{I,p} = \frac{1}{2 \langle E_I^I, H_I^I \rangle} \sum_j T_{j,p} [\langle E_j^II, H_I^I \rangle - \langle E_I^I, H_j^II \rangle]. \quad (6)$$

If the series expansion is truncated after N terms, the transmission coefficient will be calculated by solving an $N \times N$ linear system, and then the reflection coefficients will be obtained by a simple matrix multiplication. Although these coefficients are obtained upon incidence of a mode with index p , the whole procedure can be repeated using all modes p in $1 \rightarrow N$. Thereby, we will obtain the transmission and reflection matrices that completely characterize the scattering that occurs at the interface.

III. INTERFACE BETWEEN DIELECTRIC AND PHOTONIC CRYSTAL WAVEGUIDES

A. First Approach

Fig. 2(a) shows the structure under study that is formed by a dielectric waveguide butt coupled to a single-line defect photonic crystal waveguide. In this case, medium II shown in Fig. 1 is not a z -invariant medium but a periodic medium, which consists of an infinite number of repetitions of the same basic period in the z direction. Propagation in the periodic medium is determined by Bloch modes [23]. Mode properties can change significantly within the basic period. Therefore, the coupling efficiency will depend on the interface chosen among all of the possible cuts within the basic period.

In order to calculate the transmission and reflection matrices of the structure shown in Fig. 2(a), we expand the fields of medium II in terms of the Bloch modes and use (5) and (6). These equations are still valid because the orthogonality relation is invoked by using the field expansions of the dielectric waveguide, which is a z -invariant medium. It is worth mentioning that the orthogonality of Bloch modes is only true at the high symmetry points. On the other hand, only forward-propagating Bloch modes are used in the series expansion because a semi-infinite photonic crystal waveguide is considered. In order to distinguish the forward-propagating Bloch modes from the back-

ward-propagating Bloch modes, we look at the power flux for the guided mode and at the imaginary part of the wave vector for the evanescent modes [24].

In eigenmode expansion, the structure is sliced up into layers where the index profile does not change in the propagation direction. In each of these individual layers, we can write the field as a sum of the eigenmodes. In the case of Bloch modes, the field in each layer is composed of forward and backward components. Equations (5) and (6) can be simplified by expressing the Bloch modes in terms of their forward and backward components so that we obtain

$$\langle E_j^{\text{II}}, H_1^{\text{I}} \rangle = \sum_k (F_k^j + B_k^j) \cdot \langle \tilde{E}_k, H_1^{\text{I}} \rangle \quad (7)$$

$$\langle E_1^{\text{I}}, H_j^{\text{II}} \rangle = \sum_k (F_k^j - B_k^j) \cdot \langle E_1^{\text{I}}, \tilde{H}_k \rangle \quad (8)$$

where \tilde{E}_k and \tilde{H}_k are the eigenmodes of the individual layer that depend on the chosen cut position within the basic period. Adding and subtracting (7) and (8) results in

$$\begin{aligned} \langle E_j^{\text{II}}, H_1^{\text{I}} \rangle + \langle E_1^{\text{I}}, H_j^{\text{II}} \rangle &= \sum_k F_k^j \cdot \left(\langle \tilde{E}_k, H_1^{\text{I}} \rangle + \langle E_1^{\text{I}}, \tilde{H}_k \rangle \right) \\ &\quad + \sum_k B_k^j \cdot \left(\langle \tilde{E}_k, H_1^{\text{I}} \rangle - \langle E_1^{\text{I}}, \tilde{H}_k \rangle \right) \end{aligned} \quad (9)$$

$$\begin{aligned} \langle E_j^{\text{II}}, H_1^{\text{I}} \rangle - \langle E_1^{\text{I}}, H_j^{\text{II}} \rangle &= \sum_k F_k^j \cdot \left(\langle \tilde{E}_k, H_1^{\text{I}} \rangle - \langle E_1^{\text{I}}, \tilde{H}_k \rangle \right) \\ &\quad + \sum_k B_k^j \cdot \left(\langle \tilde{E}_k, H_1^{\text{I}} \rangle + \langle E_1^{\text{I}}, \tilde{H}_k \rangle \right). \end{aligned} \quad (10)$$

Substituting (9) and (10) into (5) and (6), we obtain the transmission and reflection matrices for the structure shown in Fig. 2(a), which can be expressed by the following matrix equations:

$$T = F^{-1} (I + T_{12} R_{12} T_{12}^{-1} B F^{-1})^{-1} T_{12} \quad (11)$$

$$R = (R_{12} T_{12}^{-1} F + T_{12}^{-1} B) T \quad (12)$$

where the transmission matrix can be simplified to

$$T = F^{-1} (I - R_{21}^T B F^{-1})^{-1} T_{12}. \quad (13)$$

It can be shown that T_{ij} and R_{ij} are the transmission and reflection matrices of the structure shown in Fig. 2(b), which are calculated using (5) and (6). In Fig. 2(b), the medium I-II is the individual layer corresponding to the interface chosen within the basic period of the photonic crystal. Therefore, it can be deduced that the problem shown in Fig. 2(a) can be decomposed in the two subproblems shown in Fig. 2(b) and (c) and a similar derivation can be followed to obtain the scattering matrices.

B. Second Approach

In this subsection, we demonstrate that another approach to calculate the scattering matrices of the structure shown in Fig. 2(a) is to separate the basic structure into two structures, shown in Fig. 2(b) and (c), and then combine the transmission and reflection matrices of each structure. Mediums I and I-II

are z -invariant media so that we expand the fields in terms of the eigenmodes of each medium. On the other hand, medium II is a periodic medium so that we expand the fields in terms of the Bloch modes.

In the first structure, shown in Fig. 2(b), the forward and backward propagating modes are related by a transfer matrix

$$F_{\text{I-II}} = T_{12} F_{\text{I}} + R_{21} B_{\text{I-II}} \quad (14)$$

$$B_{\text{I}} = R_{12} F_{\text{I}} + T_{21} B_{\text{I-II}} \quad (15)$$

where T_{ij} and R_{ij} are the transmission and reflection matrices calculated using (5) and (6). On the other hand, in the second structure, shown in Fig. 2(c), there are no backward-propagating Bloch modes in medium II, so that

$$F_{\text{II}} = T_{23} F_{\text{I-II}} \quad (16)$$

$$B_{\text{I-II}} = R_{23} F_{\text{I-II}}. \quad (17)$$

In this case, T_{23} and R_{23} can also be simplified by expressing the Bloch modes in terms of forward and backward components. Moreover, it can be seen that, as the interface layer of medium II is the same as that of medium I-II, the eigenmodes expansion will be the same in both media allowing us to take advantage of the orthogonality relation. Therefore, it can be shown that

$$\langle E_j^{\text{II}}, H_1^{\text{I-II}} \rangle = (F_{\text{I}}^j + B_{\text{I}}^j) \cdot \langle \tilde{E}_{\text{I}}, \tilde{H}_{\text{I}} \rangle \quad (18)$$

$$\langle E_1^{\text{I-II}}, H_j^{\text{II}} \rangle = (F_{\text{I}}^j - B_{\text{I}}^j) \cdot \langle \tilde{E}_{\text{I}}, \tilde{H}_{\text{I}} \rangle. \quad (19)$$

Thus, inserting (18) and (19) into (5) and (6), we obtain

$$T_{23} = F^{-1} \quad (20)$$

$$R_{23} = B F^{-1}. \quad (21)$$

These results are in agreement with those reported in [19] and [24] where a plane-wave expansion was used to describe the input field as well as the Bloch modes.

The transmission and reflection matrices of the full structure can be easily calculated by relating (14)–(17) and inserting (20) and (21) which yields

$$T = F^{-1} (I - R_{21} B F^{-1})^{-1} T_{12} \quad (22)$$

$$R = R_{12} + T_{21} B T. \quad (23)$$

It can be seen that the transmission matrices given by (13) and (22) are the same because $R_{21}^T = R_{21}$ due to reciprocity. Furthermore, the reflection matrices given by (14) and (23) are also identical as is demonstrated in Appendix A1.

The transmission and reflection matrices involve the scattering properties of both guided, radiation, and evanescent modes. Thus, the power transmission and reflection efficiency from the fundamental mode of the dielectric waveguide into the fundamental guided propagating Bloch mode and assuming that the modes are normalized is given by

$$\eta_T = |T_{0,0}|^2 \quad (24)$$

$$\eta_R = |R_{0,0}|^2 \quad (25)$$

where $T_{0,0}$ is the first element of (22) while $R_{0,0}$ is the first element of (23).

TABLE I
DESCRIPTION OF THE MAIN PARAMETERS OF THE TWO PHOTONIC CRYSTAL STRUCTURES CONSIDERED. n_{defects} AND n_{medium} ARE THE REFRACTIVE INDEX OF THE DEFECTS (RODS OR HOLES) AND THE SURROUNDING MEDIUM RESPECTIVELY, R IS THE DEFECT RADIUS AND f_n IS THE NORMALIZED FREQUENCY EMPLOYED TO CALCULATE THE LATTICE CONSTANT a

Structure	n_{defects}	n_{medium}	R	f_n (a/λ)	a @ $\lambda=1.55\mu\text{m}$	Polarization
Rod	3.4	1.45	0.2a	0.3	465 nm	TM
Hole	1	3.4	0.3a	0.235	364.2 nm	TE

IV. RESULTS AND DISCUSSION

A. Description of the Simulation Tools Employed and Structures Analyzed

The analytic results were obtained with a frequency-domain model based on a vectorial eigenmode expansion technique and a staircase approximation of the index profile [25]. This modeling tool CAMFR is freely available from the Internet [26]. For the photonic crystal waveguide, the Bloch modes were calculated from the eigenstates of the scattering matrix associated to the basic period. Afterwards, the field profiles and the forward and backward components of the Bloch modes were obtained at the chosen cut position within the basic period in order to calculate analytic expressions. Analytic results have been compared with simulation results. The simulated structure consists of an input dielectric waveguide butt-coupled to a semi-infinite photonic crystal waveguide, as shown in Fig. 2(a). Simulations were performed with CAMFR as well as with a finite-difference time-domain (FDTD) code [27].

Two different structures have been analyzed. The first, hereafter named rod structure, consists of a $0.5\text{-}\mu\text{m}$ -wide dielectric waveguide with a core of silica (SiO_2) and a cladding of air. The photonic crystal structure considered is a two-dimensional (2-D) triangular lattice of dielectric rods of silicon (Si) surrounded by a homogeneous dielectric medium of silica. The second, hereafter named hole structure, consists of a $0.5\text{-}\mu\text{m}$ -wide dielectric waveguide with a core of Si and a cladding of air. The photonic crystal structure in this case is a 2-D triangular lattice of air holes surrounded by a homogeneous dielectric medium of Si. The main parameters of both photonic crystal structures are summarized in Table I.

Fig. 3 shows the dispersion relations of the rod and hole photonic crystal waveguides and of the dielectric waveguides considered in each case. The dispersion relations have been obtained with the plane-wave expansion (PWE) method for the photonic crystal waveguides [28] and with CAMFR for the dielectric waveguides. For the rod structure, it can be seen that both the dielectric and the photonic crystal waveguide are single mode. The lattice constant has been calculated to get transmission at $\lambda = 1.55\ \mu\text{m}$ for the central normalized frequency of the guided mode. For the hole structure, it can be seen that the dielectric waveguide is single mode while two guided modes, with odd and even symmetries in the transversal direction, appear for the photonic crystal waveguide. The lattice constant has been calculated to get transmission at $\lambda = 1.55\ \mu\text{m}$ for a normalized frequency where only the even mode exists. However, as the dielectric waveguide mode has even symmetry, only the even mode will be excited in the photonic crystal waveguide.

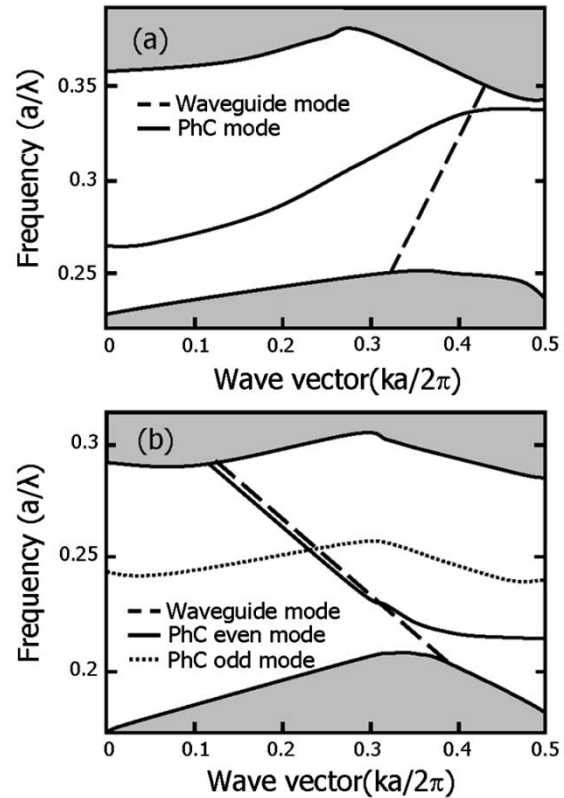


Fig. 3. Dispersion relations for the dielectric and photonic crystal waveguides in the (a) rod and (b) hole structures.

B. Coupling Efficiency Dependence on Cut Position

Coupling losses between conventional dielectric and photonic crystal waveguides are caused by the different guiding mechanism in both waveguides, which gives rise to a mode impedance mismatch. Modal properties in dielectric waveguides are unaltered along the propagation direction but, in photonic crystals, they change within the basic period that characterizes the photonic crystal. Therefore, the mode impedance mismatch between both waveguides will depend on the chosen cut position within the basic period.

Figs. 4(a) and 5(a) show the transmission efficiency as a function of the chosen cut position within the basic period normalized by the lattice constant (z/a) for the rod and hole structure, respectively. The frequency of operation is that shown in Table I. The inset of Fig. 4(a) shows the basic period considered where the propagation direction is along the z axis. It should be noticed that the cut position is only varied along the Γ K direction. Results are shown for CAMFR, FDTD, and the analytic expressions derived in Section III. It can be seen that analytic and

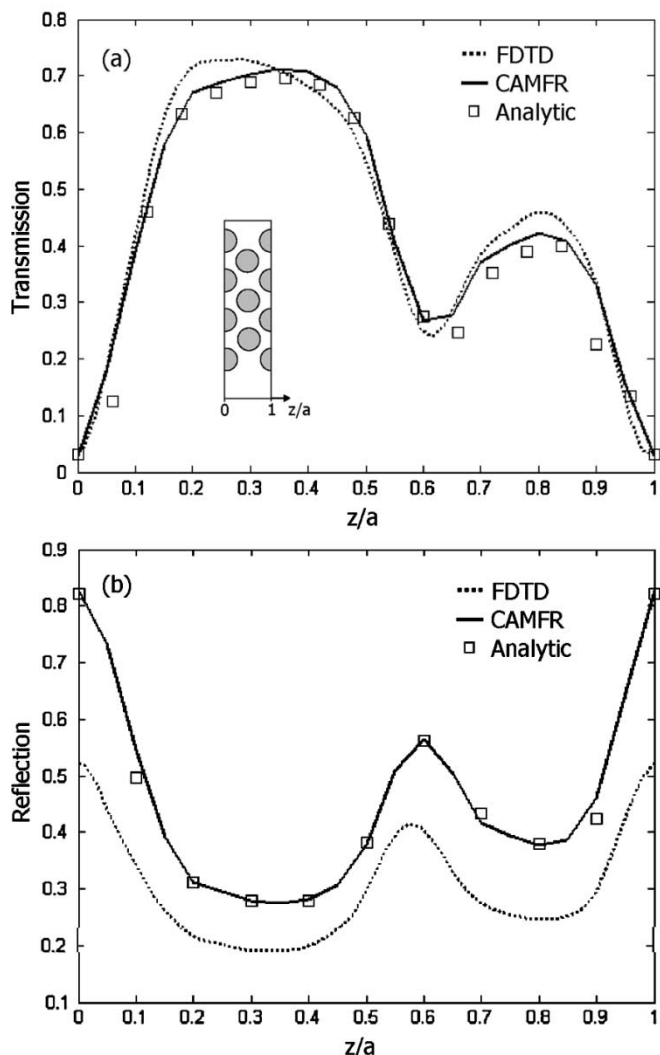


Fig. 4. (a) Transmission and (b) reflection efficiency as a function of the chosen cut position within the basic period normalized by the lattice constant (z/a) for the rod structure. The inset shows the basic period used, the propagation direction is in the z axis.

simulation results show an excellent agreement especially with CAMFR as the parameters in both simulations and analytic calculations are the same. Reflection has also been calculated and it is shown in Figs. 4(b) and 5(b) for the rod and hole structure, respectively. It can be seen that analytic and simulation results are also in agreement. However, FDTD results are something different for the rod structure. This is because, in this case, the reflection was calculated by integrating the power only along the width of the input waveguide. However, in the rod structure, as the index contrast of the dielectric waveguide is lower, the mode will be less confined and it will expand into the cladding. Therefore, the power calculation is underestimated but the shape remains unaltered.

From Figs. 4 and 5, it can be seen that the transmission response is asymmetric in both structures although the absolute value of the total field is symmetric within the basic period. This behavior can be interpreted from the transmission expression [see (22)] in which the forward and backward components of the Bloch modes are responsible for the asymmetric response as they have different values depending on the chosen cut position.

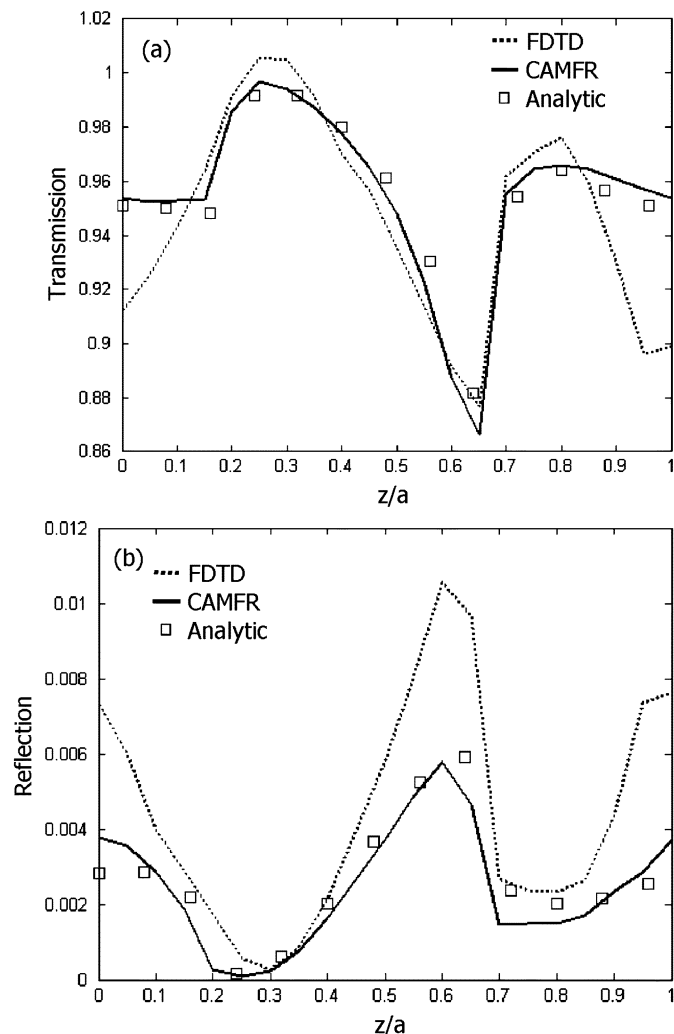


Fig. 5. (a) Transmission and (b) reflection efficiency as a function of the chosen cut position within the basic period normalized by the lattice constant (z/a) for the hole structure.

It is also interesting to notice that the transmission expression is similar to the Airy formula [29] but without any propagation terms as medium I-II has zero length. On the other hand, it can be seen that the reflection is proportional to the backward components multiplied by the transmission [see (23)]. In the hole structure, the transmission is very high while the reflection is maintained very low. Therefore, the low reflection implies that the backward components should be very low in order to counteract the high transmission.

On the other hand, a good mode profile matching is expected at the optimum cut position due to the coupling efficiency improvement. In order to show this effect, the field diagrams have been calculated at different cut positions. Fig. 6(a) and (b) shows the electric field diagrams in the rod structure for $z/a = 0.3$ and $z/a = 0.0$, respectively, which correspond to the maximum and minimum transmission efficiency shown in Fig. 4(a). Fig. 6(c) and (d) show the magnetic field diagram in the hole structure for $z/a = 0.3$ and $z/a = 0.66$, respectively, which again corresponds to the maximum and minimum transmission efficiency shown in Fig. 5(a). It can be seen that at the optimum cut position a high coupling efficiency is achieved which reflects in a

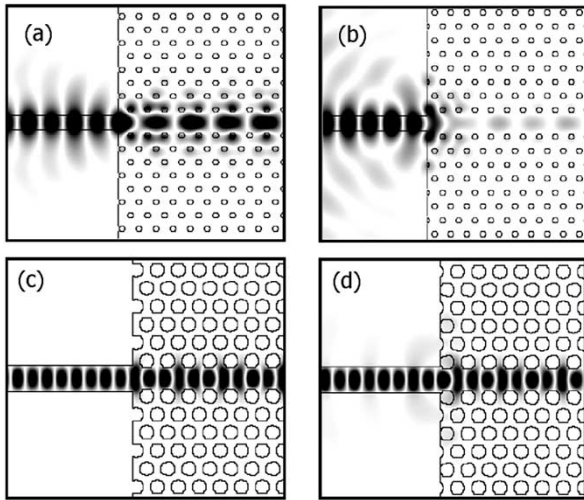


Fig. 6. Electric field diagram in the rod structure (a) $z/a = 0.3$ and (b) $z/a = 0.0$ and magnetic field diagram in the hole structure (c) $z/a = 0.3$ and (d) $z/a = 0.66$.

good mode profile matching. However, at the nonoptimum cut position, the reflection increases and the coupling efficiency decreases, which reflects in a poor mode profile matching. It is also interesting to point out that the higher reflection in the rod structure can be attributed to the fact that the waveguide mode is less confined because of the smaller index contrast which increases the mode profile mismatch. However, the reflection is also highly dependent on the modal properties of the photonic crystal waveguide, as it can be deduced from the results shown in Fig. 4, so that it cannot be stated that a more confined waveguide mode will always reduce the reflection.

C. Coupling Efficiency Dependence on Frequency

In the last section, we have seen that the transmission efficiency can be significantly improved at a fixed frequency by choosing the optimum interface. Now, we will study the dependence of transmission efficiency with frequency which is mainly determined due to the difference in the dispersion relations between the dielectric and photonic crystal waveguides. In Fig. 3(b), it can be seen that for the hole structure the dispersion relation of the dielectric and photonic crystal waveguide are very similar. This will result in an efficient coupling and high transmission will be achieved over the whole bandwidth of the photonic crystal mode. On the other hand, in the rod structure the dispersion relations of both waveguides differ more and therefore the frequency response will be worse.

Figs. 7 and 8 show the transmission spectra for the hole and rod structure, respectively, with $z/a = 0.3$ in both cases that corresponds to the optimum interface which give rise to the maximum transmission. Analytic results are compared with CAMFR and FDTD simulations, showing a good agreement. However, it can be seen that FDTD results are slightly shifted to higher frequencies especially in the rod structure. We attribute this shifting to an artifact of FDTD as the results obtained with CAMFR are also in agreement with the band diagrams shown in Fig. 3, which were calculated with the PWE method. On the other hand, the dash-dotted results shown in Figs. 7 and 8 have been calculated with the scalar Fresnel equation

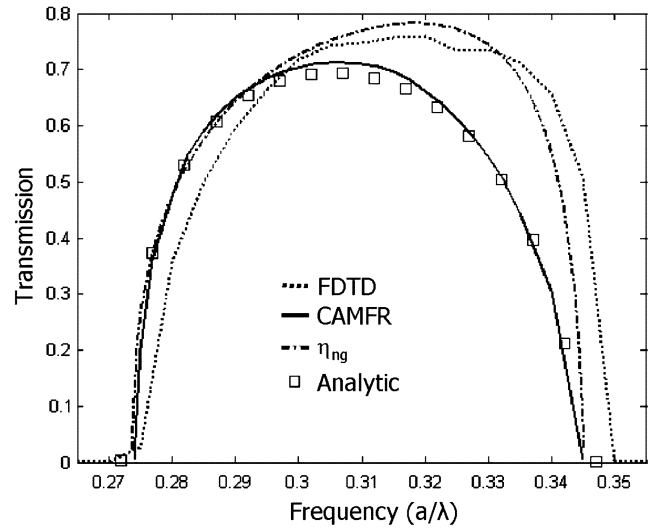


Fig. 7. Transmission efficiency as a function of the normalized frequency for the rod structure with $z/a = 0.3$.

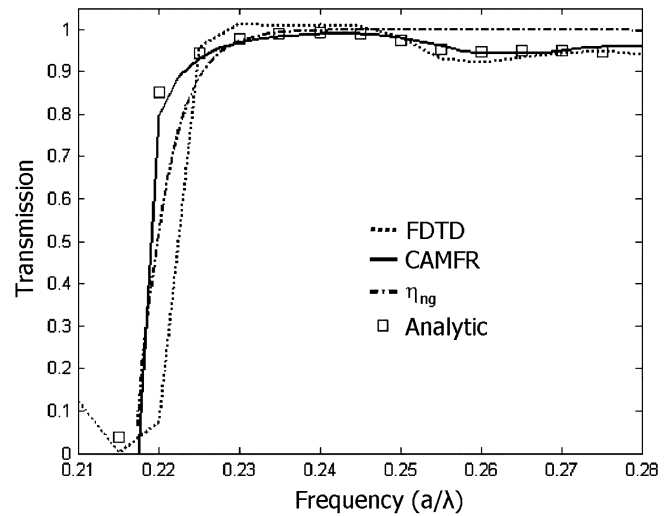


Fig. 8. Transmission efficiency as a function of the normalized frequency for the hole structure with $z/a = 0.3$.

but involving the group indexes of the dielectric and photonic crystal waveguide and are given by

$$\eta_{ng} = 4n_g^{\text{phc}}n_g^{\text{wg}} / (n_g^{\text{phc}} + n_g^{\text{wg}})^2 \quad (26)$$

where n_g^{phc} and n_g^{wg} are the group index of the photonic crystal and dielectric waveguides, respectively. The group index is inversely related to the group velocity and the group velocity is determined by the variation of the frequency with respect to the wave vector, i.e., the slope of the dispersion relation. Therefore, the group indexes can be easily calculated from the dispersion curves.

From the results presented in Figs. 7 and 8, it can be seen that the transmission spectrum presents a parabolic shape in the rod structure while it is relatively flat in the hole structure. In both cases, it is very remarkable to notice that, even though the optimum cut position has been obtained for a fixed frequency, the transmission spectrum shape is similar to the one obtained with (26), indicating that the transmission efficiency dependence with frequency mainly stems from the difference in

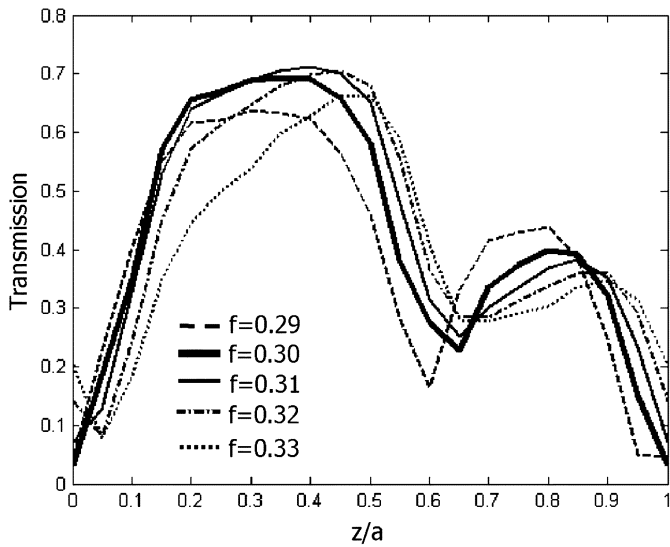


Fig. 9. Transmission efficiency as a function of the chosen cut position within the basic period normalized by the lattice constant (z/a) for the rod structure and for different normalized frequencies.

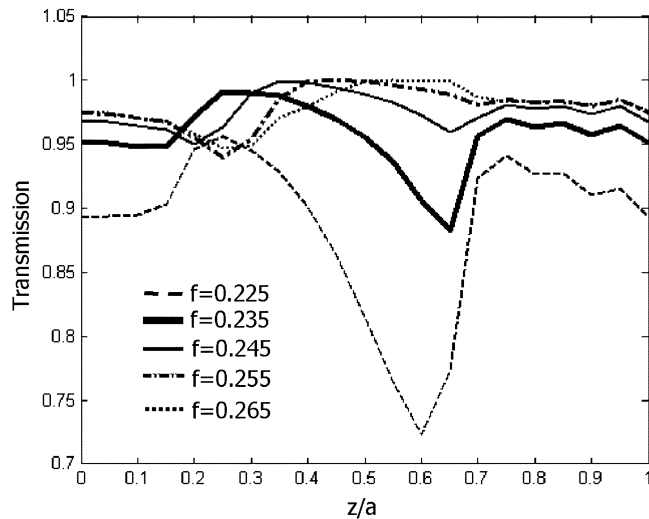


Fig. 10. Transmission efficiency as a function of the chosen cut position within the basic period normalized by the lattice constant (z/a) for the hole structure and for different normalized frequencies.

group velocity or, in other words, due to the group index mismatch. However, the influence of the frequency on the cut position has also been analyzed.

Figs. 9 and 10 show the transmission efficiency as a function of the cut position for the rod and hole structures, respectively, and considering different frequencies. Results have only been calculated with the analytic expression showing the advantages of the developed formulation as the calculation time was significantly reduced. In both structures, it can be seen that the transmission response does not change significantly with frequency and the optimum cut position is only slightly shifted. It is interesting to notice that the maximum transmission efficiency in all cases is similar to that predicted with (26). On the other hand, it can be seen that the transmission efficiency variation with the chosen cut position in the hole structure increases as the frequency is close to the band edge. In the next section, we will show that this behavior can be partly explained by looking at the forward and backward components of the fundamental guided Bloch mode.

D. Differences Between Rod and Hole Structures

We have seen in the last subsections that the coupling is much better for the hole structure rather than for the rod structure. As already mentioned, coupling losses between dielectric and photonic crystal waveguides are derived from the different guiding mechanism in the two waveguides. In the dielectric waveguide, the guiding mechanism relies only on the index-contrast effect. On the other hand, the guiding mechanism in the photonic crystal is determined by the propagation of Bloch modes. In principle, the properties of the guided Bloch mode are due to distributed Bragg reflections, but they can also be affected by the total internal reflection effect depending on the features of the photonic crystal [30], [31]. In the hole structure, the core refractive index of the photonic crystal waveguide is higher than the surrounding medium. In this case, the properties of the Bloch mode will be affected by the total internal reflection effect so that the modal properties in the dielectric and photonic crystal waveguides will be more similar, yielding a highly efficient coupling. This explains the similarity of the dispersion relations shown in Fig. 3(b). On the other hand, the photonic crystal waveguide in the rod structure has a core refractive index smaller than the surrounding medium. In this case, the guided mode is considered to be a pure Bloch mode because only the photonic bandgap (PBG) effect is present and modal properties in the dielectric and photonic crystal waveguides will differ more, yielding a worse coupling. However, we have seen that the transmission efficiency in the rod structure is highly dependent on the chosen cut position with values that go from lower than 5% to near 70%. On the other hand, the transmission efficiency variation with the chosen cut position in the hole structure is very low with values near 100%, although it increases if frequencies close to the band edge are considered. In order to give an explanation of this behavior, we have analyzed the forward and backward components of the fundamental guided Bloch mode.

The following factor for the forward component has been defined:

$$\gamma_{FW} = \frac{|\langle E_{FW}, H_{FW}^* \rangle|}{|\langle E_{FW}, H_{FW}^* \rangle| + |\langle E_{BW}, H_{BW}^* \rangle|} \quad (27)$$

where the subscripts FW and BW denote the forward and backward components of the total field, respectively. A similar expression has been used for the backward component. Fig. 11 shows the factor values as a function of the chosen cut position within the basic period normalized by the lattice constant for the rod and hole structures. Results are only shown for the frequency of operation shown in Table I for the sake of simplicity. A strong interaction between forward and backward components can be seen in the rod structure that gives rise to a large difference between the Bloch mode and the waveguide mode. Thereby, the mode profiles in the dielectric and photonic crystal waveguide are rather different, as it is shown in Fig. 6(a), so that a higher mode mismatch exists which increases reflection and scattering. The results shown in Fig. 11(a) are only related with the fundamental Bloch mode. However, the increase of scattering means that coupling losses are also determined due to interaction with higher order modes. Therefore, clear correspondence between the results shown in Figs. 11(a) and 4 cannot be seen. On the other hand, it can be seen that the Bloch mode in the hole structure is mainly determined by the forward component. Furthermore,

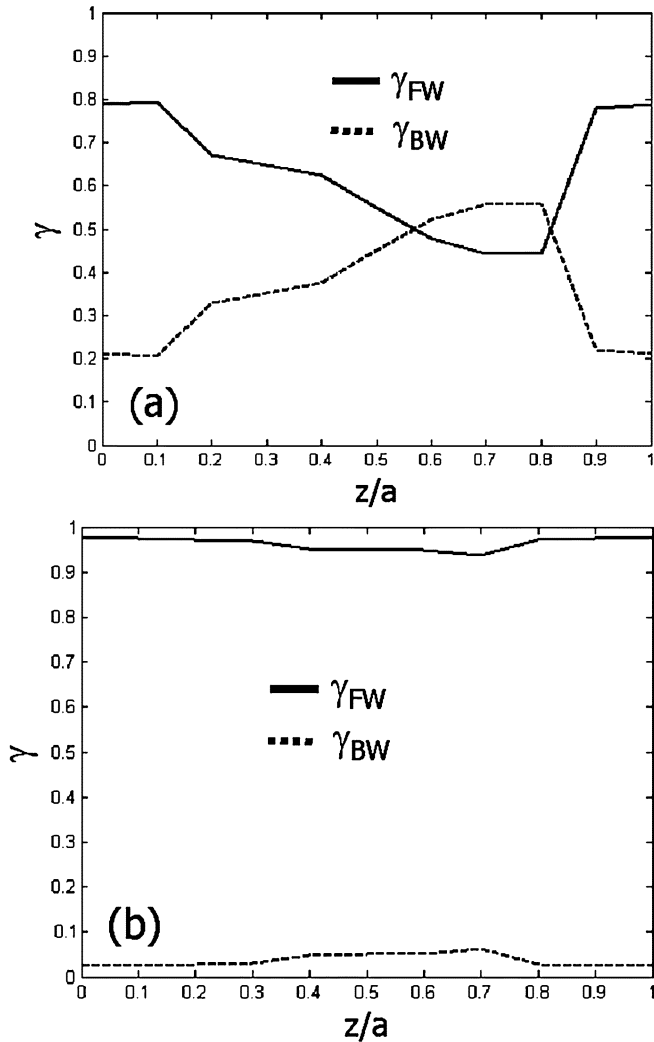


Fig. 11. Influence of forward and backward components as a function of the cut position within the basic period normalized by the lattice constant (z/a) for the (a) rod and (b) hole structures.

the γ_{FW} and γ_{BW} values are mainly constant along different cut positions within the basic period, which explains the low dependence of the transmission efficiency with the chosen cut position shown in Fig. 5(a). We attribute this behavior to the total internal reflection effect that results in a large similarity between the Bloch mode and the waveguide mode. This similarity can also be shown in the mode profiles shown in Fig. 6(c) and explains the results reported in [31], where it was shown that the properties of the photonic crystal waveguide can be similar to those obtained from an effective corrugated waveguide.

For different frequencies, we obtained similar curves for both rod and hole structures. In the latter, we observed that, for frequencies close to the band edge, the reduction of the transmission efficiency as well as the higher variation with the chosen cut position, shown in Fig. 10, was associated with an increase of the backward components, indicating a higher mode mismatch. However, we noticed that the reflection was maintained at a very low value, indicating that coupling losses mainly arose due to scattering. Therefore, the steep dip, shown in Fig. 10 and accentuated for frequencies close to the band edge, can be attributed to the complex interplay between mode mismatch and interaction with higher order modes.

E. Relation to Approximate Formulas

Finally, we also studied the usefulness of the classical approximate formula employed to study fiber-coupling issues (see, e.g., [32]) for interfaces involving photonic crystal structures. The general expression of this formula is given by

$$\eta = \frac{\text{Re}\{\langle E_I, H_{II}^* \rangle \langle E_{II}, H_I^* \rangle / \langle E_{II}, H_{II}^* \rangle\}}{\text{Re}\{\langle E_I, H_I^* \rangle\}} \quad (28)$$

where Re denotes the real part.

First, it is important to point out that this formula was successfully used to study radiation losses of a structure formed between a dielectric waveguide and a semi-infinite Bragg mirror [18]. In this case, the nonpropagating fundamental Bloch mode operating in the bandgap was considered and it was obtained that the reflection of the structure could be calculated as η^2 but using the forward field of Bloch mode instead of the total field. The proof of this assessment is beyond the scope of this paper, however, the fact of using only the forward field to calculate η^2 can be understood from (20) that shows that the transmission only involves the forward components when the input waveguide has the same index profile as the first layer of the photonic crystal waveguide, as occurs in [18].

In our case, we have analyzed the usefulness of (28) in order to calculate the transmission efficiency in the rod and hole structures. Unlike the work in [18], the transmission in this case relies on the fundamental guided propagating Bloch mode. In Appendix A2, it is demonstrated how (28) can also be obtained following the derivation presented in Section II when mediums I and II are z -invariant. In principle, this derivation is not valid when medium II is a photonic crystal because the orthogonality relation is not true if the cross product is taken with the forward field of the Bloch mode. This implies that the coupling to higher order Bloch modes in addition to the backward components of the fundamental Bloch mode should be negligible to ensure the validity of the formula. This result can be interpreted by looking at the forward and backward components of the fundamental guided Bloch mode. As previously shown, the fundamental guided Bloch mode in the hole structure is mainly determined by the forward components, however, a stronger interaction between the forward and backward components exists in the rod structure. Furthermore, a high transmission is achieved in the former case so that the coupling to higher order Bloch modes as well as the reflection can be neglected. Therefore, we conclude that, only in very specific cases, (28) can be used for coupling issues in photonic crystals.

V. CONCLUSION

Coupling losses have been analyzed at an interface formed by a dielectric waveguide butt coupled to a photonic crystal waveguide. The main contribution of the paper is the derivation of closed-form expressions for the reflection and transmission matrices that completely characterize the scattering that occurs at the interface. Analytic expressions are based on an eigenmode expansion technique but the same derivation can be used with other field expansions. Furthermore, we showed that the classical approximate formula employed to study fiber-coupling issues can only be used for interfaces involving photonic crystal structures in very specific cases.

A similar procedure to the one followed here can be derived to analyze other coupling problems. Furthermore, it is important to mention that although in this paper we have considered a 2-D problem for the sake of simplicity, analytic expressions are also valid in three-dimensional (3-D) problems. Therefore, they can be a useful instrument in order to study coupling issues in 3-D avoiding highly consuming resources and complex simulations.

In a second step, analytic expressions, validated by means of CAMFR and FDTD simulations, were used to analyze coupling losses in two different photonic crystal structures. We showed that the transmission efficiency can be significantly improved by choosing the optimum cut position within the basic period of the photonic crystal. Thereby, the transmission efficiency can be increased from values lower than 5% to values near 70% for the rod structure while efficiency near 100% can be achieved for the hole structure. On the other hand, we obtained that, even choosing the optimum interface, the maximum transmission efficiency is limited by the group velocity mismatch. Finally, we showed that the behavior of the coupling efficiency can be partly predicted by analyzing the forward and backward components of the guided propagating Bloch mode.

APPENDIX A

DEMONSTRATION OF THE REFLECTION MATRICES EQUALITY

In this Appendix, it is demonstrated that (12) is equivalent to (23), which is defined by

$$R = R_{12} + T_{21}BT. \quad (A1)$$

First, we can put (A1) into the form

$$R = (R_{12}T_{12}^{-1}(I - R_{21}BF^{-1})F + T_{21}B)T. \quad (A2)$$

After some algebraic manipulations, we obtain

$$R = (R_{12}T_{12}^{-1}F + T_{12}^{-1}(T_{12}T_{21} + R_{21}R_{21})B)T \quad (A3)$$

where it can be shown that

$$T_{12}T_{21} + R_{21}R_{21} = I \quad (A4)$$

by using the self-inverting property of the scattering matrix and relating it with the transfer matrix [22]. Thus, it can be shown that (A3) is equal to (12).

APPENDIX B

APPROXIMATE FORMULA FOR THE POWER COUPLING EFFICIENCY IN z -INVARIANT MEDIA

The approximate formula usually employed to study fiber-coupling issues can also be derived from (1) and (2). In this case, the reflection is neglected and the transmission is obtained by taking the right cross product of (1) with H_I^{II} and the left cross product of (2) with E_I^{II} . However, as the reflection has been neglected, the transmission efficiencies obtained from (1) and (2) will be different, as follows:

$$\langle E_p^{\text{I}}, H_I^{\text{II}} \rangle = \sum_j T_{j,p}^E \langle E_j^{\text{II}}, H_I^{\text{II}} \rangle \quad (B1)$$

$$\langle E_I^{\text{II}}, H_p^{\text{I}} \rangle = \sum_j T_{j,p}^H \langle E_I^{\text{II}}, H_j^{\text{II}} \rangle. \quad (B2)$$

The transmission from the incident mode into the desired transmitted mode is obtained using the orthogonality relation in (B1) and (B2) which yields

$$T_E = \langle E_I, H_{\text{II}} \rangle / \langle E_{\text{II}}, H_{\text{II}} \rangle \quad (B3)$$

$$T_H = \langle E_{\text{II}}, H_I \rangle / \langle E_{\text{II}}, H_{\text{II}} \rangle. \quad (B4)$$

The power coupling efficiency is then described by

$$\eta = \frac{\text{Re}\{T_E T_H^* \langle E_{\text{II}}, H_{\text{II}}^* \rangle\}}{\text{Re}\{\langle E_I, H_I^* \rangle\}}. \quad (B5)$$

However, the above derivation is normally followed by using the conjugated magnetic field, which gives rise to the same results provided we have lossless materials. Thus, (B5) results in

$$\eta = \frac{\text{Re}\{\langle E_I, H_{\text{II}}^* \rangle \langle E_{\text{II}}, H_I^* \rangle / \langle E_{\text{II}}, H_{\text{II}}^* \rangle\}}{\text{Re}\{\langle E_I, H_I^* \rangle\}}. \quad (B6)$$

In conventional index-guiding waveguides, the tangential component of the magnetic and electric fields are related by the wave impedance, allowing us to simplify (B7) into the well-known formula

$$\eta = \frac{|\langle E_I, E_{\text{II}}^* \rangle|^2}{\langle E_I, E_I^* \rangle \langle E_{\text{II}}, E_{\text{II}}^* \rangle}. \quad (B7)$$

REFERENCES

- [1] J. D. Joannopoulos, R. D. Meade, and N. J. Winn, *Photonic Crystals: Molding the Flow of Light* Princeton, NJ, Sept. 1995.
- [2] S. John, "Strong localization of photons in certain disordered superlattices," *Phys. Rev. Lett.*, vol. 8, pp. 2486–2489, 1987.
- [3] E. Yablonovitch, "Inhibited spontaneous emission in solid-state physics and electronics," *Phys. Rev. Lett.*, vol. 58, pp. 2059–2062, 1987.
- [4] T. D. Happ, M. Kamp, and A. Forchel, "Photonic crystal tapers for ultracompact mode conversion," *Opt. Lett.*, vol. 26, pp. 1102–1104, 2001.
- [5] P. Sanchis, J. Martí, A. García, A. Martínez, and J. Blasco, "High efficiency coupling technique for planar photonic crystal waveguides," *Electron. Lett.*, vol. 38, pp. 961–962, Aug. 2002.
- [6] —, "Mode matching technique for highly efficient coupling between dielectric waveguides and planar photonic crystal circuits," *Opt. Express*, vol. 10, pp. 1391–1397, Dec. 2002.
- [7] A. Talneau, M. Mulot, S. Anand, and Ph. Lalanne, "Compound cavity measurements of transmission and reflection of a tapered single-line photonic crystal waveguide," *Appl. Phys. Lett.*, vol. 82, pp. 2577–2579, 2003.
- [8] P. Pottier, I. Ntakis, and R. M. De La Rue, "Photonic crystal continuous taper for low-loss direct coupling into 2D photonic crystal channel waveguides and further device functionality," *Optics Communications*, vol. 223, pp. 339–347, 2003.
- [9] P. Bienstman, S. Assefa, S. G. Johnson, J. D. Joannopoulos, G. S. Petrich, and L. A. Kolodziejski, "Taper structures for coupling into photonic crystal slab waveguides," *J. Opt. Soc. Am. B*, vol. 20, pp. 1817–1821, 2003.
- [10] R. Stoffer, H. Hoekstra, R. M. De Ridder, E. V. Groesen, and F. P. H. Van Beckum, "Numerical studies of 2D photonic crystals: Waveguides, coupling between waveguides and filters," *Opt. Quantum. Electron.*, vol. 32, pp. 947–961, 2000.
- [11] A. Mekis and J. D. Joannopoulos, "Tapered couplers for efficient interfacing between dielectric and photonic crystal waveguides," *IEEE J. Lightwave Technol.*, vol. 19, pp. 861–865, 2001.
- [12] A. Adibi, X. Yong, R. K. Lee, A. Yariv, and A. Scherer, "Properties of the slab modes in photonic crystal optical waveguides," *J. Lightwave Technology*, vol. 18, pp. 1554–1564, Nov. 2000.
- [13] M. Qiu, K. Azizi, A. Karlsson, M. Swillo, and B. Jaskorzynska, "Numerical studies of mode gaps and coupling efficiency for line-defect waveguides in two-dimensional photonic crystals," *Phys. Rev. E*, vol. 64, 2001. 155 113.
- [14] E. Miyai, M. Okano, M. Mochizuki, and S. Noda, "Analysis of coupling between two-dimensional photonic crystal waveguide and external waveguide," *Appl. Phys. Lett.*, vol. 81, pp. 3729–3731, 2002.
- [15] N. Moll and G. L. Bona, "Comparison of three-dimensional photonic crystal slab waveguides with two-dimensional photonic crystal waveguides: Efficient butt coupling into these photonic crystal waveguides," *J. Appl. Phys.*, vol. 93, pp. 4986–4991, 2003.

- [16] E. Silberstein, P. Lalanne, and J. P. Hugonin, "Use of grating theories in integrated optics," *J. Opt. Soc. Am. A*, vol. 18, pp. 2865–2875, 2001.
- [17] Ph. Lalanne and J. P. Hugonin, "Bloch-wave engineering for high Q 's, small V 's microcavities," *IEEE J. Quantum. Electron.*, vol. 39, pp. 1430–1438, 2003.
- [18] M. Palamaru and P. Lalanne, "Photonic crystal waveguides: Out-of-plane losses and adiabatic modal conversion," *Appl. Phys. Lett.*, vol. 78, pp. 1466–1468, 2001.
- [19] L. C. Botten, A. A. Asatryan, T. N. Langtry, T. P. White, C. Martijn de Sterke, and R. C. McPhedran, "Semianalytic treatment for propagation in photonic crystal waveguides," *Opt. Lett.*, vol. 28, no. 10, pp. 854–859, 2003.
- [20] S. G. Johnson, P. Bienstman, M. A. Skorobogatiy, M. Ibanescu, E. Lidorikis, and J. D. Joannopoulos, "Adiabatic theorem and continuous coupled-mode theory for efficient taper transitions in photonic crystals," *Phys. Rev. E*, vol. 66, p. 066 608, 2002.
- [21] K. A. Zaki, S. Chen, and C. Chen, "Modeling discontinuities in dielectric-loaded waveguides," *IEEE Trans. Microwave Theor. Tech.*, vol. 36, pp. 1804–1810, 1988.
- [22] G. V. Eleftheriades, A. S. Omar, L. P. B. Katehi, and G. M. Rebeiz, "Some important properties of waveguide junction generalized scattering matrices in the context of the mode matching technique," *IEEE Trans. Microwave Theor. Tech.*, vol. 42, pp. 1896–1903, 1994.
- [23] F. Bloch, "Über die quantenmechanik der electronen in kristallgittern," *Z. Physik*, vol. 52, pp. 555–600, 1928.
- [24] L. C. Botten, N. A. Nicorovici, R. C. McPhedran, C. Martijn de Sterke, and A. A. Asatryan, "Photonic band structure calculations using scattering matrices," *Phys. Rev. E*, vol. 64, 2001. 046 603.
- [25] P. Bienstman, "Rigorous and Efficient Modeling of Wavelength Scale Photonics Components," Ph.D. Dissertation, Ghent Univ., Ghent, Belgium, 2001.
- [26] , <http://camfr.sourceforge.net>.
- [27] A. Taflove, *Computational Electrodynamics*. Norwood, MA: Artech, 1995.
- [28] S. G. Johnson and J. D. Joannopoulos, "Block-iterative frequency-domain methods for Maxwell's equations in a planewave basis," *Opt. Express*, vol. 8, pp. 173–190, 2001.
- [29] P. Yeh, *Optical Wave in Layered Media*. New York: Wiley, 1988.
- [30] S. G. Johnson, P. R. Villeneuve, S. H. Fan, and J. D. Joannopoulos, "Linear waveguides in photonic-crystal slabs," *Phys. Rev. B*, vol. 62, pp. 8212–8222, 2000.
- [31] A. Adibi, Y. Xu, R. K. Lee, M. Loncar, A. Yariv, and A. Scherer, "Role of distributed Bragg reflection in photonic-crystal optical waveguides," *Phys. Rev. B*, vol. 64, 2001. 041 102(R).
- [32] E. J. Murphy, "Fiber attachment for guided devices," *IEEE J. Light. Tech.*, vol. 6, pp. 862–871, June 1988.



Pablo Sanchis (S'01) was born in Valencia, Spain, in 1978. He received the degree in telecommunications engineering from Universidad Politécnica de Valencia, Valencia, Spain, in 2001, where he is currently working toward the Ph.D. degree.

In 2003, he spent six months with the Photonics Research Group of the Department of Information Technology, Ghent University. He is member of the Radio over Fiber Group of the Valencia Nanophotonics Technology Center, Universidad Politécnica de Valencia. His research interests include modeling,

design, and fabrication issues in integrated optics, especially in the field of photonic crystals. He has published several papers and holds one patent.



Peter Bienstman (S'97–A'01) was born in Ghent, Belgium, in 1974. He received the degree in electrical engineering and the Ph.D. degree from Ghent University, Ghent, Belgium, in 1997 and 2001, respectively.

He currently holds a postdoctoral position with the Department of Information Technology (INTEC), Ghent University. During 2001–2002, he spent a year in the Joannopoulos research group at the Massachusetts Institute of Technology, Cambridge. His research interests include the modeling of optical structures, notably photonic crystal structures,

vertical-cavity surface-emitting lasers, and resonant-cavity light-emitting diodes. He has published several papers and holds one patent.

Dr. Bienstman is a member of the IEEE Lasers and Electro-Optics Society.



Electro-Optics Society.

Bert Luyssaert (M'01) was born in Ghent, Belgium, in 1976. He received the degree in physics and the degree in engineering physics from Ghent University, Ghent, Belgium, in 1998 and 2000, respectively, where he is currently working toward the Ph.D. degree in engineering.

His research interests include design and fabrication of components for microphotonics and, in particular, coupling problems between various components.

Mr. Luyssaert is member of the IEEE Lasers and



Roel Baets (M'88–SM'96) received the degree in electrical engineering from Ghent University, Ghent, Belgium, in 1980, the M.Sc. degree in electrical engineering from Stanford University, Stanford, CA, in 1981, and the Ph.D. degree from Ghent University in 1984.

Since 1981, he has been with the Department of Information Technology (INTEC), Ghent University. Since 1989, he has been a Professor on the engineering faculty of Ghent University. From 1990 to 1994, he was also a part-time Professor

with the Technical University of Delft, Delft, The Netherlands. He has mainly worked in the field of photonic components. With about 300 publications and conference papers as well as about 10 patents he has made contributions to the design and fabrication of III-V semiconductor laser diodes, passive guided wave devices, photonic integrated circuits, and microoptic components. He leads the Photonics Group at Ghent University-INTEC (which is an associated lab of IMEC), working on photonic devices for optical communication and optical interconnect.

Dr. Baets is a member of the Optical Society of America, the IEEE Lasers and Electro-Optics Society (LEOS), SPIE, and the Flemish Engineers Association. He has been member of the program committees of OFC, ECOC, IEEE Semiconductor Laser Conference, ESSDERC, CLEO-Europe, IPR, and the European Conference on Integrated Optics. He has been chairman of the IEEE-LEOS Benelux chapter from 1999 to 2001. Currently he is a member of the Board of Governors of IEEE LEOS.



Javier Martí (S'89–M'92) received the Ingeniero de Telecomunicación degree from the Universidad Politécnica de Catalunya, Catalunya, Spain, in 1991, and the Doctor Ingeniero de Telecomunicación degree (Ph.D.) from the Universidad Politécnica de Valencia, Valencia, Spain, in 1994.

During 1989 and 1990, he was an Assistant Lecturer with the Escuela Universitaria de Vilanova, Barcelona, Spain. From 1991 to 2000, he was a Lecturer and Associate Professor with the Telecommunication Engineering Faculty, where he

is currently a Professor and leads the Radio over Fiber Group. Recently, he was appointed Director of the Valencia Nanophotonics Technology Centre. He has authored or coauthored over 120 papers in referred international technical journals and over 60 papers in international conference proceedings in the fields of broad-band hybrid fiber-radio systems and microwave/millimeter-wave photonics, fiber-based access networks, terabit/s OTDM/WDM optical networks, advanced optical processing techniques for microwave signals and ultrahigh-speed data transmission and planar photonic crystals.

Prof. Martí has served as member of the Technical Program Committee of ECOC, Microwave Photonics, and other international workshops and conferences.